



Full Length Article

Calibration of Superconducting Radio-Frequency cavity forward and reflected channels based on stored energy dynamics[☆]Andrea Bellandi^{ID*}, Julien Branlard, Marco Diomedè, Max Herrmann, Sven Pfeiffer^{ID}, Christian Schmidt

Deutsches Elektronen-Synchrotron DESY, Notkestraße. 85, 22607, Hamburg, Germany

ARTICLE INFO

Keywords:

LLRF
Signal calibration
Superconducting RF
Accelerating cavities

ABSTRACT

Modern superconducting radio-frequency linear accelerators require the cavity bandwidth and detuning to be within a specified range to maximize the efficiency of the machine. To correctly estimate these states during operation, the measured RF signals should be calibrated. Due to the finite isolation of the waveguide directional couplers, cross-coupling effects in the forward and reflected channels complicate the calibration of the RF signals in Low-Level RF control systems. Past work proposed a compensation method employing least-squares optimization. This method requires the directivity of the directional couplers to be much higher than one. Additionally, the algorithm requires a tuning parameter to optimize the calculated calibration. However, for some accelerating systems, finding an acceptable value for such a parameter is challenging and time-consuming. Other methods strongly depend on the forward-reflected ratio during the field decay phase. This, in some circumstances, may decrease the accuracy due to noise or systematic errors. In this paper, we present a way to overcome these limitations by performing a global nonlinear least square optimization constrained by energy conservation laws. The method is tested with L-band superconducting resonators at loaded quality factors of $4.6 \cdot 10^6$ and $2.8 \cdot 10^7$.

1. Introduction

The task of continuously estimating the state of Superconducting Radio-Frequency (SRF) cavities is essential for the efficient operation of linear particle accelerators. The cavity unloaded quality factor or Q_0 is related to the losses dissipated in the cryogenic system

$$P_{cryo} = \frac{U}{\omega_0 Q_0}, \quad (1)$$

with P_{cryo} the dissipated power, U the stored electromagnetic energy inside the RF cavity and ω_0 the cavity resonance in angular frequency [1]. Q_0 is related to the cavity half bandwidth $\omega_{1/2}$

$$\omega_{1/2} = \frac{\omega_0}{2} \left(\frac{1}{Q_0} + \frac{1}{Q_{ext}} \right) = \frac{\omega_0}{2Q_L}, \quad (2)$$

with Q_{ext} the external quality factor, which describes the coupling strength between the superconducting cavity and the transmission line used to transfer power from the RF amplifier to the resonator. Q_L is the loaded quality factor. Assuming Q_{ext} to be constant during operations, the variations in cryogenic heat losses can be estimated by measuring $\omega_{1/2}$. It is also assumed $Q_0 \gg Q_{ext}$ during nominal operation. Therefore

a cavity quench, that reduces Q_0 by several orders of magnitude, makes $\omega_{1/2}$ deviating from $\approx \frac{\omega_0}{2Q_{ext}}$. A protection system needs to shut the RF drive as soon as a variation of $\omega_{1/2}$ is detected to prevent excessive heat dissipation in the cryogenic system. When not caught, quenches can result in increased downtime or, in extreme cases, in damages to the cryogenic system [2]. In short pulse particle accelerators like European XFEL (EuXFEL) [3], this can be accomplished by measuring the time constant of the RF field decay. However, for Continuous Wave (CW) or pulsed machines with a duty factor of several ten percent, alternative methods have to be used.

Another important parameter that needs to be estimated in real-time is the cavity detuning $\Delta\omega$. Such a parameter describes the difference between the frequency of the high-power driving signal and the cavity resonance frequency. For on-crest acceleration, detuning increases the required power P_{RF} needed to drive an RF resonator at a certain voltage [4]

$$P_{RF} = \frac{|V_P|^2}{4 \frac{r}{Q} Q_L} \left[\left(1 + \frac{\frac{r}{Q} Q_L I_b}{|V_P|} \right)^2 + \frac{\Delta\omega^2}{\omega_{1/2}^2} \right], \quad (3)$$

[☆] Work supported by European XFEL GmbH.

* Corresponding author.

E-mail address: andrea.bellandi@desy.de (A. Bellandi).



Fig. 1. S.P.A. FERRITE, WDHC 3-3A bi-directional coupler for 1.3 GHz waveguides. The declared directivity is 40 dB.

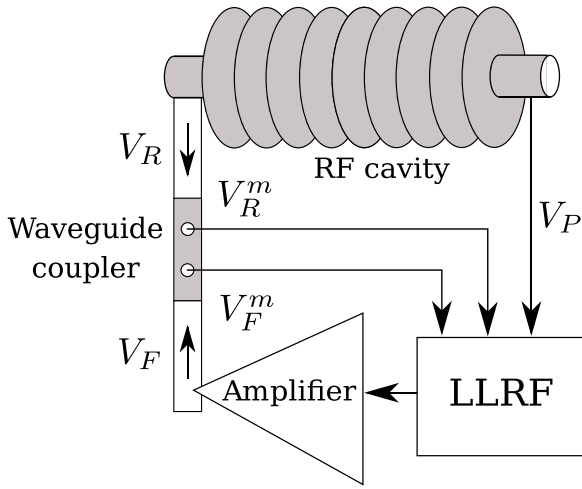


Fig. 2. Simplified RF cavity-based accelerating system. A waveguide connects the high-power amplifiers to the cavity. On the waveguide, a bidirectional coupler is used to sample the forward V_F and reflected V_R RF components.

where r/Q is the shunt impedance and $V_p \in \mathbb{C}$ is the accelerating voltage or *calibrated probe signal* and I_b the beam current. The real and imaginary parts of V_p represent respectively the In-phase and Quadrature (I&Q) components. Estimating and correcting for $\Delta\omega$ during operations maximizes the efficiency of the accelerator. The efficient operation of the RF cavities results also in a reduction in cost and size of the RF amplifiers.

Already since years, FPGA-based LLRF control systems are capable of calculating $\Delta\omega$ and $\omega_{1/2}$ in real-time using model-based approaches [5,6]. To perform the estimation, the measured RF cavity probe and forward signals are used. However, imperfections in the RF measurement chain result in errors in the estimated states. One of the most important systematic error in the measurements arises from waveguide directional couplers (Fig. 1) used to sample the forward (V_F) RF signal sent from the RF high-power amplifier and reflected (V_R) wave at the cavity power coupler. Since these devices have a finite directivity, the measured signals V_F^m and V_R^m are affected by the opposite components (Fig. 2). This effect is particularly strong when the directional couplers are placed between the cavity coupler and the circulator. In other schemes, the waveguide coupler for the

forward signal is placed between the amplifier and the circulator while the waveguide coupler for the reflected signal is placed between the circulator and the RF dump. In this case, the isolation of the circulator determines the cross-coupling between V_F and V_R . In both cases, to correct the measured signals for cross-coupling effects, it is necessary to apply a calibration matrix as described in [7,8]

$$V_F = aV_F^m + bV_R^m \quad (4)$$

$$V_R = cV_F^m + dV_R^m \quad (5)$$

where $a, b, c, d \in \mathbb{C}$ represent the signal calibration of V_F and V_R . For the model of (4) and (5), it is assumed that the directional coupler behaves as a linear device. In principle, with an accurate RF characterization of the whole chain, it would be possible to estimate the parameters of (4) and (5). However, in practice, this procedure might be excessively time-consuming, error-prone, and affected by drifts like the humidity and temperature dependence of RF cables.

2. Discussion on the current methods for signal calibration

Another way to estimate a, b, c, d is to characterize the accelerating system by relying completely on the measurements performed by the LLRF system. Assuming V_p is already calibrated using beam-based methods or by RF power-based methods, the simplest form of calibration can be performed using a general result from the physics of transmission lines

$$V_p(n) = V_F(n) + V_R(n) \quad \forall n \in N, \quad (6)$$

where N is the set of the indices of the recorded data samples. Eq. (6) states that the sum of the forward and reflected waves at the end of the transmission line is equal to the voltage on the termination load which, in this case, is the SRF cavity. It is important to point out that, using (6), V_F and V_R are not defined anymore as the amplitude of the RF signals in the waveguide. Instead, V_F and V_R now represent the transformed voltages when considering the cavity power coupler as an electrical transformer [1]. The advantage of such a decision is that, while still having calibrated values proportional to the RF fields in the waveguide, it avoids requiring the parameters of the cavity power coupler in the equations. Under these considerations, (4) and (5) still hold.

2.1. Diagonal calibration

If the effect of the finite directivity is negligible for the intended application, the non-diagonal terms b, c of (4) and (5) can be set to zero and only a, d are used. It is then possible to find the diagonal terms of the over-determined system of (6) using a least square optimization for linear systems [9].

2.2. Calibration from Pfeiffer et al.

If the effect of the directivity on the measurements makes the use of the diagonal calibration method not viable, all the parameters of (4) and (5) have to be used. This results in (6) being not constrained enough and having an infinite number of solutions for a, b, c, d . A way to solve this issue is presented in [7] by Pfeiffer et al. This method requires the data to represent an RF pulse in the SRF resonator. The data is then divided into two parts

$$N = N_{pulse} \cup N_{decay}, \quad (7)$$

with N_{pulse} the set of the indices when the amplifier that excites the cavity is generating an RF signal and N_{decay} the set of indices when the same amplifier is switched off and the cavity field follows an unforced decay. Then additional constraints are added

$$V_F(n) = 0 \quad \forall n \in N_{decay}, \quad (8)$$

$$V_R(n) = V_p(n) \quad \forall n \in N_{decay}. \quad (9)$$

Eqs. (8) and (9) state that the forward signal V_F is equal to zero during the decay period and, as a consequence of (6), the reflected signal V_R is equal to the probe signal. The above constraints turn out to be too strict, since the measurement noise results in (6) to be solved only for $a, b = 0$. Having an RF calibration that results in $V_F(n) = 0 \quad \forall n \in N$ is physically meaningless. Therefore additional constraints are added to penalize the magnitude of $|b|, |c|$. These constraints can be strengthened by adjusting the weighing parameter k_{add} .

Even though the above method has shown to be effective and reliable in calibrating cavity signals at EuXFEL, some limitations might prevent its practical application in other facilities:

1. The suggested procedure is to evaluate the calibration with $k_{add} = 1$. If the computed calibration is not satisfactory, the calibration should be repeated at different values of the parameter. Then, the result that minimizes the standard variation of the estimated cavity bandwidth on the calibrated signals is chosen. Such an operation is time-consuming and, at certain facilities (e.g. at the ELBE accelerator at Helmholtz Zentrum Dresden-Rossendorf [10]) the algorithm is not able to estimate the calibration parameters in a stable and reliable manner.
2. The procedure assumes the ratio

$$|S_{ab}| \simeq \frac{1}{|N_{decay}|} \sum_{n \in N_{decay}} \left| \frac{V_F^m(n)}{V_R^m(n)} \right| \ll 1. \quad (10)$$

Therefore (10) requires the directivity of the waveguide couplers to be much smaller than unity. This might not be true for every facility.

3. Systems that show a significant reflection of V_R back to the cavity are not expected to fulfill (10). This may happen, for example, if a mismatched RF element is present in the waveguide system.

2.3. Calibration from A. Brandt

Another possible method is discussed by A. Brandt [8]. The b, c, d parameters are written as functions of a

$$b(a) = \frac{a}{z}, \quad (11)$$

$$c(a) = x - a, \quad (12)$$

$$d(a) = y - \frac{a}{z}, \quad (13)$$

The parameters x and y are respectively the a_{diag} and d_{diag} calibration coefficients determined using the diagonal method. z is the solution of the over-determined linear system

$$z = \frac{a}{b} = -\frac{V_R^m(n)}{V_F^m(n)} \quad \forall n \in N_{decay}. \quad (14)$$

With (11), (12) and (13) only a needs to be found. To calculate the value of a , an optimization problem is given in [8]

$$a = \arg \min_a \sum_{n \in N} \left(\frac{d|V_P(n)|}{dt} + \omega_{1/2}(|V_P(n)| - \Re\{\frac{\overline{V_P(n)}}{|V_P(n)|} V_F(n; \hat{a})\}) \right)^2. \quad (15)$$

It is assumed that $\omega_{1/2}$ is known and constant during the RF pulse used in the calibration. $V_F(n; \hat{a})$ represents the calibrated forward signal using a certain value of a and the condition of (11). In [8] it is prescribed to calculate (15) assuming an initial value $\hat{a} = a_{diag}$ and then using a minimization routine until the convergence of \hat{a} to a .

One possible limitation of Brandt's method is that it depends on the value of z . Therefore the precision of measurement of $V_F^m(n)$ during the decay phase has an impact on the final calibration. Since the magnitude of $V_F^m(n)$ during the decay is proportional to b , the signal might be dominated by noise or systematic errors thus negatively affecting the calibration.

2.4. Calibration from F. Qiu et al.

F. Qiu et al. [11] proposed a variation of A. Brandt's method to track calibration drifts in CW operation. In the paper it is assumed that the value of z is known beforehand and is constant over time since it only depends on the directional coupler S-parameters. Then, in closed loop RF operation

$$\frac{dV_P(n)}{dt} \simeq 0 \quad \forall n \in N. \quad (16)$$

Using the condition in (16) it is possible to derive the optimization problem

$$a = \arg \min_a \sum_{n \in N} \left| \frac{V_F(n; \hat{a})}{V_P(n)} - \frac{1}{2} \right| \quad (17)$$

Since in this paper only calibration algorithms that require a pulsed RF structure are compared, no further discussion will be done on the method of Qiu et al.

3. Derivation of the energy-based calibration method

To overcome the limitations of the above methods, we present a new calibration procedure that is based on the superconducting cavity system dynamics. Unlike Brandt's method, the whole set of calibration parameters (a, b, c, d) is used in the optimization to remove the algorithm dependency over z . Using the RF cavity equation in complex form [12]

$$\frac{dV_P}{dt} = -(\omega_{1/2} + j\Delta\omega)V_P + 2\omega_{1/2}V_F. \quad (18)$$

In (18) $\Delta\omega$ is unknown and generally time-varying. Then, $\overline{V_P}$ is multiplied on both sides of (18). By taking the real part of (18), an equation that describes the dynamics of the stored energy inside the cavity and does not depend on $\Delta\omega$ is derived

$$\frac{1}{2\omega_{1/2}} \frac{d|V_P(n)|^2}{dt} + |V_P(n)|^2 = 2\Re\{\overline{V_P(n)}V_F(n)\}, \quad (19)$$

$\forall n \in N.$

From (19), the optimization problem of (15) can be derived by expressing it in terms of a and minimizing the difference of its right and left side. Instead, the non-differentiated terms of V_P are substituted with (6)

$$\frac{1}{2\omega_{1/2}} \frac{d|V_P(n)|^2}{dt} = |V_F(n)|^2 - |V_R(n)|^2 \quad \forall n \in N. \quad (20)$$

Since (20) depends only on the square of the signals, it can be interpreted as an energy conservation condition. Eq. (20) states that the variation in the stored electromagnetic energy is equal to the difference between the forward and reflected power. Apparently, deriving (20) is not necessary since (6) and (19) implicitly describe the energy conservation of the system. Moreover, using (20) requires solving an over-determined nonlinear system of equations. However, it is found that not using (20) results in an insufficiently constrained magnitude of the cross-coupling term of the reflected signal and, as a consequence, decreases the accuracy of the calculated calibration parameters. Therefore it is possible to formulate an optimization problem to find a, b, c, d

$$(a, b, c, d) = \arg \min_{\hat{a}, \hat{b}, \hat{c}, \hat{d}} \left(\sum_{n \in N} (|f_{probe}(n; \hat{a}, \hat{b}, \hat{c}, \hat{d})|^2 + |f_C(n; \hat{a}, \hat{b}, \hat{c}, \hat{d})|^2 + |f_D(n; \hat{a}, \hat{b})|^2) \right). \quad (21)$$

The terms f_{probe}, f_C, f_D represent the errors given by subtracting the left and right sides of (6), (20), and (19). These terms are defined as

$$f_{probe}(n; \hat{a}, \hat{b}, \hat{c}, \hat{d}) = V_F(n; \hat{a}, \hat{b}) + V_R(n; \hat{c}, \hat{d}) - V_P(n), \quad (22)$$

$$f_C(n; \hat{a}, \hat{b}, \hat{c}, \hat{d}) = \frac{|V_F(n; \hat{a}, \hat{b})|^2 - |V_R(n; \hat{c}, \hat{d})|^2 - C(n)}{\max_{n \in N} |V_P(n)|}, \quad (23)$$

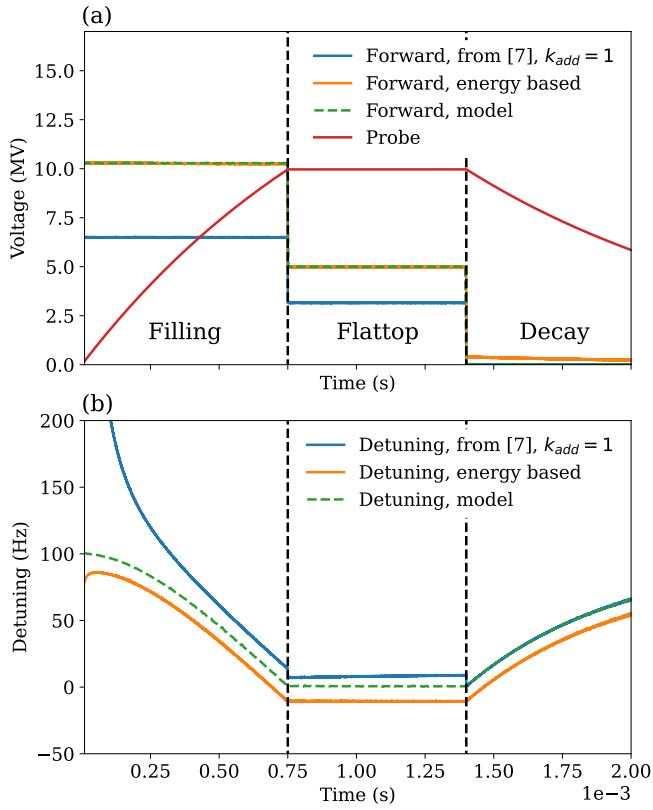


Fig. 3. Comparison of different calibration methods with respect to the simulated model. The measurement noise is removed. The probe and forward cavity signals (a) and the estimated detuning (b) are displayed. The model calibration coefficients are $|a| = 0.976$, $|b| = 0.145$, $|c| = 0.207$, $|d| = 0.879$. Therefore, the condition $|S_{ab}| \ll 1$ of [7] is not fulfilled. The *Energy* method shows an offset in the detuning and an incorrect nonzero amplitude of the forward signal during the decay phase. These effects justify the addition of 8 from [7] to the *Energy* optimization (21).

$$f_D(n; \hat{a}, \hat{b}) = \frac{2\Re\{\overline{V_P(n)}V_F(n; \hat{a}, \hat{b})\} - D(n)}{\max_{n \in N} |V_P(n)|}, \quad (24)$$

$$C(n) = \frac{1}{2\omega_{1/2}} \frac{d|V_P(n)|^2}{dt}, \quad (25)$$

$$D(n) = C(n) + |V_P(n)|^2, \quad (26)$$

where (23) and (24) are normalized to the maximum amplitude of the probe signal to have the same units as (22). The problem described by (21) can be solved to calculate a, b, c, d . For this, the *least_squares* routine of the package SciPy [13] is used to numerically find the minimum of (21).

4. Simulations

Multiple sets of simulations are performed to evaluate the performance of the algorithm described in the previous section. The model for the simulations is a 1.3 GHz TESLA-like [14] cavity with a half bandwidth $\omega_{1/2} = 2\pi \cdot 141.3$ Hz as for the EuXFEL accelerator. The pulse structure is chosen to have an initial *filling* period of 750 μ s with $V_F = 10.28$ MV. After the filling period a *flattop* period of 650 μ s at $V_F = 5.00$ MV results in a steady state gradient $V_P = 10$ MV. Finally, a *decay* period of 600 μ s with $V_F = 0$ ends the pulse. To add a realistic detuning profile, a predetuning of 100 Hz and a Lorentz Force Detuning (LFD) component equal to -1 Hz(MV) $^{-2}$ is added to the simulation. The detuning $\Delta\omega$ is then

$$\Delta\omega(V_P(t)) = 2\pi(100 - 1 \cdot |V_P(t)|^2). \quad (27)$$

Table 1

Normalized RMSE bandwidth and detuning estimation errors over $\omega_{1/2}$ for the $|S_{ab}| \approx -40$ dB case.

Method	nRMSE($\omega_{1/2}^e$) %	nRMSE($\Delta\omega^e$) %
None	7.89	8.27
Diagonal	7.52	8.15
From [7], $k_{add} = 1$	5.80	6.07
A. Brandt	0.15	1.63
Energy	0.07	19.05
Energy constr.	0.08	0.97

Eq. (18) is used to simulate the system with the chosen parameters with a sample rate $f_s = 10$ MHz. A Gaussian measurement noise with $\sigma_n = 1$ kV is added to the simulated traces when evaluating the calibration algorithm. A Gaussian actuator noise with $\sigma_a = 10$ kV is also added to represent the oscillations in the output signal of the amplifier. An example of a simulated cavity pulse with the above parameters is given in Fig. 3(a).

For the algorithm in [7], it is prescribed to start with $k_{add} = 1$ and then vary it to optimize the calibration. However, attempts of varying k_{add} often result in unsatisfactory local minima in the calibration correctness. Therefore, since [7] does not describe how to perform such a parametric optimization, it is decided to keep $k_{add} = 1$. This choice could result in an unfair comparison with the other methods, but, on the other hand, it puts all the algorithms roughly at the same level in terms of time for executing a single calibration. Additionally, this algorithm is always run with $k_{add} = 1$ when used for calibrating EuXFEL or FLASH. Therefore, the use of $k_{add} = 1$ is still representative of the calibration accuracy of the algorithm compared with how the algorithm itself is used under current operating conditions.

For the energy based and A. Brandt's algorithm, (15), (19) and (20) require to compute $\omega_{1/2}$, $\frac{d|V_P(n)|}{dt}$ and $\frac{d|V_P(n)|^2}{dt}$. To take into account the effect of σ_n in real scenarios, it is decided to estimate $\omega_{1/2}$ in each simulation by doing an exponential fit of $|V_P(n)|$ on the decay period. To compute $\frac{d|V_P(n)|}{dt}$ and $\frac{d|V_P(n)|^2}{dt}$ a Savitzky-Golay derivator routine from [13] is used. The parameters used in *savgol_filter* are a window length of 201 and a filter order of 3. This results in a signal bandwidth approximately equal to 62 kHz [15]. Filtering and deriving the square amplitude of the probe signal results in distortions of the computed trace around the transition between the filling and flattop and the transition between the flattop and decay. Therefore 201 samples, equal to the filtering window, are removed from N before and after the transition points at the end of the filling and flattop regions. Three simulated datasets with normally distributed values for a, b, c, d are generated:

1. $|S_{ab}| \approx -40$ dB: in this dataset it is assumed that the conditions of the method from Pfeiffer et al. are fulfilled. A randomly distributed contribution with $\sigma_c = 0.01$ is set on a, b, c, d in every simulation. The average of a, d is $\mu_{a,d} = 1$, while, for b, c $\mu_{b,c} = 0$.
2. $|S_{ab}| \approx -20$ dB: in this dataset $\sigma_c = 0.1$
3. $|S_{ab}| \approx -40$ dB with randomly distributed predetuning: in this dataset $\sigma_c = 0.01$. The cavity is simulated with an additional detuning component, applied from the beginning of the pulse to its end, which is normally distributed with $\sigma_{det} = 260$ Hz through the different elements of the dataset.

Each dataset contains 1024 different cavity simulations. The calibration algorithms are executed on each element of the datasets. Then, the computed coefficients are used to calibrate the denoised cavity signals and estimate the cavity half bandwidth $\omega_{1/2}^e(n)$ and detuning $\Delta\omega^e(n)$ traces. The Root Mean Square Error (RMSE) normalized to $\omega_{1/2}$ of $\omega_{1/2}^e(n)$, $\Delta\omega^e(n)$ with respect to the underlying model is used to evaluate the goodness of the different calibration procedures. Additionally, the average absolute error on each calibration parameter is calculated. For the $|S_{ab}| \approx -40$ dB dataset, Table 1 shows that the algorithm

Table 2

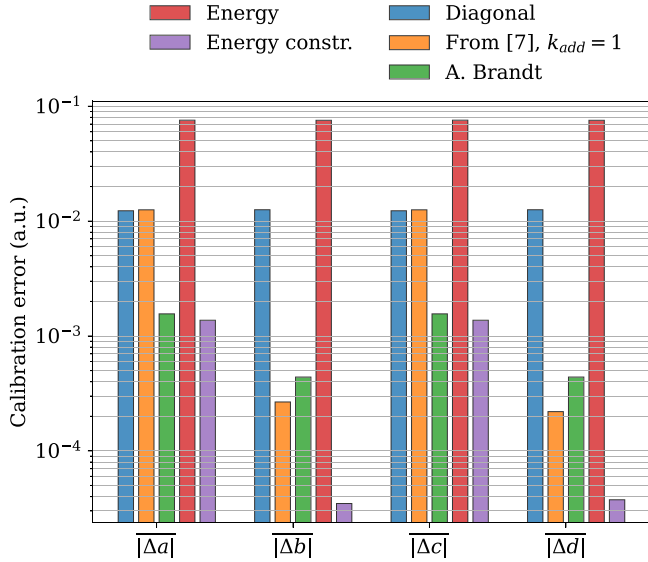
Normalized RMSE bandwidth and detuning estimation errors over $\omega_{1/2}$ for the $|S_{ab}| \approx -20$ dB case.

Method	nRMSE($\omega_{1/2}^e$) %	nRMSE($\Delta\omega^e$) %
None	79.95	86.27
Diagonal	76.86	83.67
From [7], $k_{add} = 1$	102.35	63.17
A. Brandt	0.03	0.46
Energy	0.08	21.37
Energy constr.	0.08	0.97

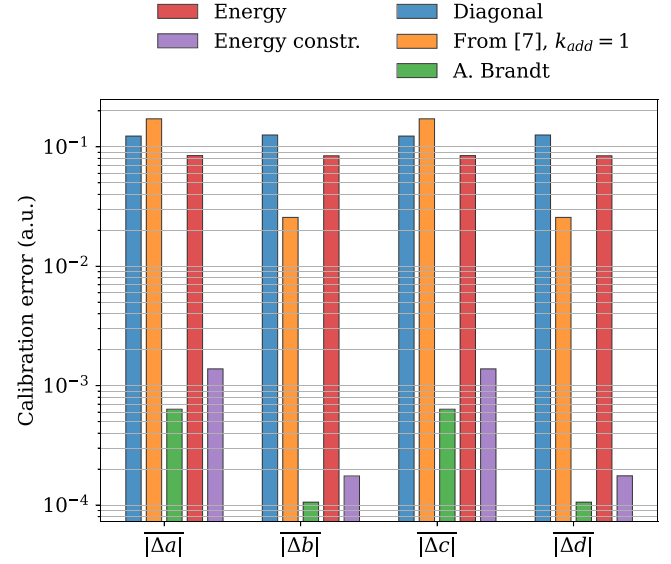
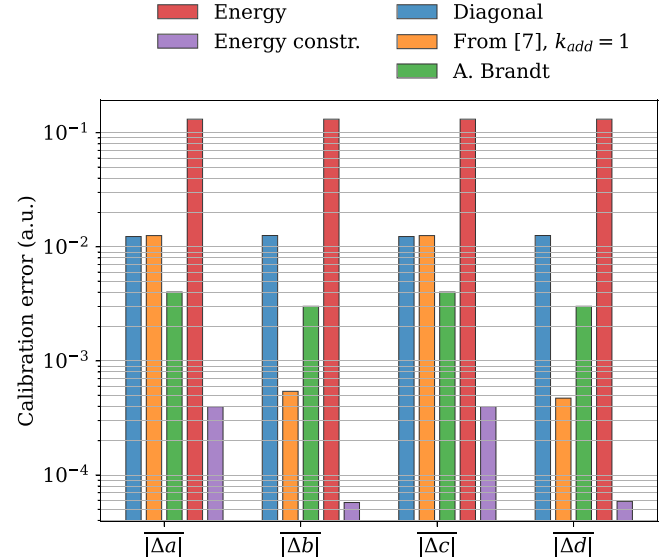
Table 3

Normalized RMSE bandwidth and detuning estimation errors over $\omega_{1/2}$ for the $|S_{ab}| \approx -40$ dB with randomly distributed predetuning case.

Method	nRMSE($\omega_{1/2}^e$) %	nRMSE($\Delta\omega^e$) %
None	7.98	8.37
Diagonal	7.69	8.27
From [7], $k_{add} = 1$	5.93	6.18
A. Brandt	3.23	8.36
Energy	0.05	33.89
Energy constr.	0.05	0.38

**Fig. 4.** Average errors on the a, b, c, d parameters for the $|S_{ab}| \approx -40$ dB dataset.

from [7] results in the reduction of roughly 2% nRMSE compared to the uncompensated case. A. Brandt's method achieves excellent calibration results with an nRMSE of 0.15% for the bandwidth and 1.63% for the detuning. The diagonal calibration method does not result in a significant nRMSE improvement. The energy calibration, even if results in only a 0.07% nRMSE for the half bandwidth computation, results in an error for the detuning twice as big as the uncorrected case. Fig. 4 shows that for the energy calibration, the average error on the a, b, c, d parameters is the highest among all the calibration methods. This result hints that the energy-based method is insufficiently constrained. Then, the $|S_{ab}| \approx -20$ dB dataset is analyzed (Fig. 5). In Table 2 the error for the detuning and bandwidth measured for the diagonal method and the one from [7] is comparable to $\omega_{1/2}$ and only slightly better than the uncorrected case. This comes with no surprise since these methods are suited for small to zero values for b, c . For the A. Brandt's method, the nRMSE is 0.03% for the bandwidth and 0.46% for the detuning. For the energy-based method, the errors on detuning and bandwidth for the $|S_{ab}| \approx -20$ dB dataset are similar to the $|S_{ab}| \approx -40$ dB case. Further qualitative investigations on the detuning and bandwidth give an explanation for such a behavior. Fig. 3(b) shows that, even though the energy calibration resulted in an estimated detuning trace

**Fig. 5.** Average errors on the a, b, c, d parameters for the $|S_{ab}| \approx -20$ dB dataset.**Fig. 6.** Average errors on the a, b, c, d parameters for the $|S_{ab}| \approx -40$ dB with randomly distributed predetuning dataset.

that matches the shape of the detuning model, it presents a constant difference between the two traces. The algorithm from [7] shows a detuning trace that significantly deviates from the model in the filling and flattop period but matches it in the decay period. A similar behavior is found in all the analyzed simulations. This finding motivates a modification of the original version of the calibration algorithm. The constrain of (8) is included to (21). This *energy constrained* calibration method improves the detuning estimation by reducing the nRMSE($\omega_{1/2}^e$) to less than 1%, with a precision of the same order of magnitude of A. Brandt's method. The energy constrained algorithm always performs better than the other methods when evaluating the $|S_{ab}| \approx -40$ dB with randomly distributed predetuning case. While for the other algorithms, the nRMSE for detuning and bandwidth is similar or worse than the simple $|S_{ab}| \approx -40$ dB case, the energy-constrained method improves the estimations with respect to the other cases (Fig. 6, Table 3). Even when compared to A. Brandt's method, the energy constrained method achieves more than an order of magnitude higher in terms of precision.

Table 4

nRMSE of the estimated bandwidth with different calibrations at CMTB, EuXFEL, and AMTF. CMTB and EuXFEL are equipped with 1.3 GHz accelerating cavities.

Method	nRMSE($\overline{\omega_{1/2}^e}$) %	
	EuXFEL	CMTB
None	7.05	14.64
Diagonal	4.39	13.66
From [7], $k_{add} = 1$	2.04	13.90
A. Brandt	0.50	0.32
Energy constr.	0.75	0.31

5. Measurements on SRF cavity systems

Measurements are carried out at EuXFEL and at the CryoModule Test Bench (CMTB) [16]. Each facility allows to test the algorithms with different cavity conditions. In real machines, as opposed to simulations, it is not possible to know the ground truth for the detuning estimation. Therefore, the goodness of the calibration algorithms is evaluated only by computing the systematic estimation errors on the bandwidth flatness. However, since there might be other systematic errors on the measurement chain other than the finite directivity of the waveguide couplers, the data analysis only gives a lower bound on the precision of the algorithm. For the analysis, 1024 traces were acquired for each facility. The first of these traces is used to calculate the a, b, c, d parameters. Then, the obtained parameters are used to calibrate all the other measured traces. The estimated $\omega_{1/2}^e$ is used to calculate the normalized RMSE($\overline{\omega_{1/2}^e}$) defined as

$$\text{nRMSE}(\overline{\omega_{1/2}^e}) = \frac{1}{\omega_{1/2}^{(0)}} \sqrt{\frac{\sum_{n \in N} \left(\sum_{m=1}^M \frac{\omega_{1/2}^{e(m)}(n) - \omega_{1/2}^{(m)}}{M} \right)^2}{|N|}}, \quad (28)$$

where $\omega_{1/2}^{e(m)}(n)$ represents the estimated model-based bandwidth of the m th collected trace and $\omega_{1/2}^{(m)}$ is calculated using the decay. Since, from the previous section, there are no clear benefits in using the original version of the energy-based calibration method with respect to its constrained version, we decide to just use the improved algorithm in the analysis of the experimental data.

5.1. EuXFEL

The measurements at EuXFEL are performed on a TESLA cavity with a $Q_L = 4.6 \cdot 10^6$ equivalent to a half bandwidth of $\omega_{1/2} = 2\pi \cdot 141.3$ Hz. The tests are performed in a closed radio-frequency loop in Generator Driven Resonator (GDR) mode of operation with $\max_{n \in N} |V_P(n)| = 22.6$ MV. The filling length is $750 \mu\text{s}$, while the flattop length is $650 \mu\text{s}$. The expected directivity of the waveguide couplers is in the order of 40 dB. Fig. 7 shows the estimated bandwidth and detuning traces for a single pulse. For the chosen cavity, the energy constrained method gives $|a| = 0.981$, $|b| = 0.021$, $|c| = 0.015$, $|d| = 0.994$. Therefore, for this cavity, the $|S_{ab}| \ll 1$ condition is roughly valid. This is confirmed by the results listed in Table 4. The method from Pfeiffer et al. improves the error of the $\text{nRMSE}(\overline{\omega_{1/2}^e})$ with respect to the uncorrected and diagonal case by a factor roughly 3 and 2 respectively. The energy-constrained method improves the error with respect to the uncorrected case by a factor of 10 and by a factor of 2.7 with respect to Pfeiffer et al. When compared to A. Brandt's method, the energy-constrained method achieve a similar precision.

5.2. CMTB

As for the EuXFEL case, the measurements at CMTB are performed on a TESLA cavity. Q_L is set to $2.8 \cdot 10^7$ equivalent to $\omega_{1/2} = 2\pi \cdot 22.5$ Hz.

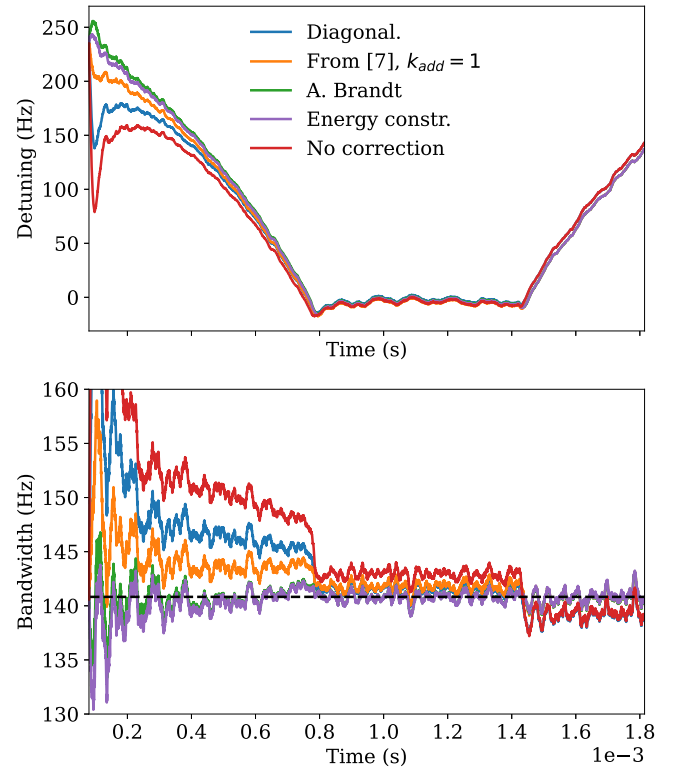


Fig. 7. Detuning (a) and bandwidth (b) for the EuXFEL cavity, calculated with different calibrations. The measurements are taken with a closed RF loop. The resonator is a 1.3 GHz TESLA cavity with $Q_L = 4.6 \cdot 10^6$.

The tests are performed in an open radio-frequency loop in GDR mode of operation with $\max_{n \in N} |V_P(n)| = 10.6$ MV. The filling length is $750 \mu\text{s}$, while the flattop length is $650 \mu\text{s}$. With the energy constrained method $|a| = 1.05$, $|b| = 0.038$, $|c| = 0.122$, $|d| = 0.960$. The high value for $|c|$ suggests that the method from Pfeiffer et al. would not perform well in calibrating this cavity. This is qualitatively confirmed by Fig. 8 and numerically in Table 4. Evaluating the bandwidth with the uncorrected and diagonal methods gives similar results in terms of achieved error. Contrary to this trend, the energy-constrained algorithm performs even better than the EuXFEL case with an nRMSE of 0.31%. Also in this case, A. Brandt's method performs similarly to the energy-constrained method.

6. Conclusion

In this paper, a new method to calibrate the forward and reflected signal of a superconducting cavity is exposed. The algorithm assumes a finite directivity of the waveguide couplers used to sample the forward and reflected signals and corrects it. While the presented method performs a multi-dimensional complex optimization of all the calibration parameters using physical Eqs. (21), the methods found in literature either use a constraint on the magnitude of the cross-coupling parameters ((10) from [7]) or rewrite the b, c, d coefficients in function of a to perform a single complex variable optimization ((15) for the algorithm from [8]). From the simulations and the experiments performed, the algorithm always results in a calibration error for the bandwidth and detuning of less than 1% nRMSE. In some cases, the signals calibrated with the new method are one order of magnitude or more more precise than with the other approaches. Particularly interesting are the measurements performed on a high- Q_L cavity at CMTB. Here, the model-based half bandwidth has an RMSE of just 0.07 Hz when averaging the estimations over multiple pulses. Therefore these results might open new possibilities in using model-based

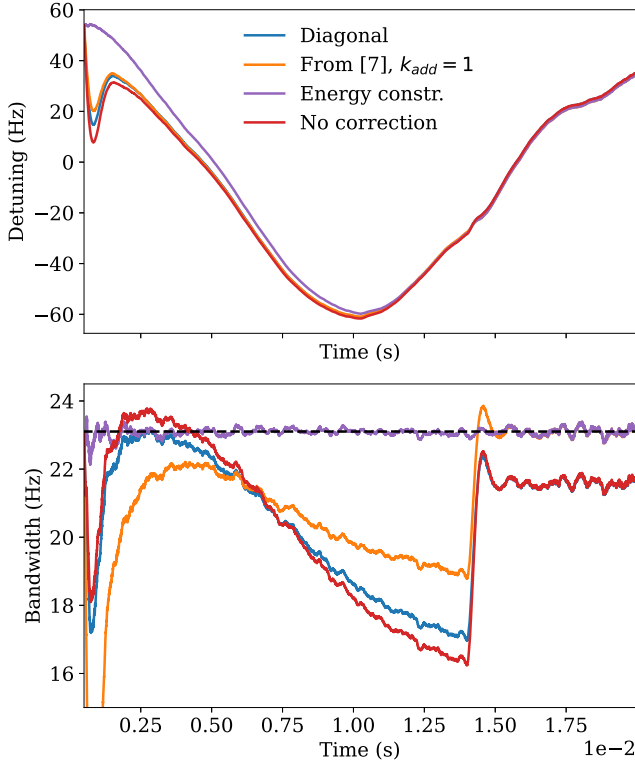


Fig. 8. Detuning (a) and bandwidth (b) for the CMTB cavity, calculated with different calibrations. The measurements are taken with an open RF loop. The resonator is a 1.3 GHz TESLA cavity with $Q_L = 2.8 \cdot 10^7$. A. Brandt's method is not shown since it results in traces that overlap the energy-constrained ones.

techniques to reliably perform quench detection when a sufficiently low-noise, low-drift LLRF measurement chain is used. Additionally, this technique is particularly useful in high Q_L accelerating systems that require an Hz-scale precision in the compensation of the detuning. Some additional work has to be carried out to examine how the technique behaves in the presence of a mismatched element that generates a driving signal even when the RF amplifier is switched off. In this case, initial evaluations show that the algorithm is able to extrapolate the equivalent cavity model including the frequency, Q_L , and phase shift generated by the reflective component (see Appendix A). However, it has still to be seen what the consequences are when this reflective element has time-changing properties. Such a situation can occur, for example in Vector-Sum (VS) systems with poor isolation on the circulators. In this case, all the other cavities can perform as variable reflective elements depending on their detuning state. In most of the cases A. Brandt's method performs similarly to the presented algorithm. However, simulations suggest that A. Brandt's method may perform poorly in cases when the calibration is performed on detuned cavities. For the algorithm of [7], the tuning parameter is kept as $k_{add} = 1$. Therefore, the results presented in this paper are not representative of the performances of the algorithm of [7] if an optimization of k_{add} is performed. Finally, the approaches presented in this paper and in A. Brandt do not have a closed mathematical form but are given as an optimization problem. This can potentially result in a sub-optimal solution depending on the minimization algorithm used. However, this issue was not observed so far and the methods behave always in a reliable and reproducible manner. In Appendix B, a Python implementation of the algorithm is given, along with a version of all the other algorithms used in this study.

CRediT authorship contribution statement

Andrea Bellandi: Writing – original draft, Software, Methodology, Investigation, Formal analysis, Data curation, Conceptualization. **Julien Branlard:** Writing – review & editing, Writing – original draft, Validation, Supervision, Project administration, Funding acquisition. **Marco Diomede:** Investigation, Data curation. **Max Herrmann:** Writing – review & editing, Resources, Data curation. **Sven Pfeiffer:** Writing – review & editing, Software. **Christian Schmidt:** Writing – review & editing, Resources, Data curation.

Declaration of competing interest

The authors declare the following financial interests/personal relationships which may be considered as potential competing interests: Andrea Bellandi reports financial support was provided by European X-Ray Free-Electron Laser Facility GmbH. Marco Diomede reports financial support was provided by European X-Ray Free-Electron Laser Facility GmbH. Max Herrmann reports financial support was provided by European X-Ray Free-Electron Laser Facility GmbH. If there are other authors, they declare that they have no known competing financial interests or personal relationships that could have appeared to influence the work reported in this paper.

Data availability

Data will be made available on request.

Acknowledgments

We want to thank B. Yildirim and V. Katalev for the information provided for the 1.3 GHz waveguide directional coupler.

Appendix A. Calibration in presence of waveguide reflections

Since the constraint of (8) imposes V_F to be equal to zero in the decay period, it is interesting to understand what is the consequence of this choice in systems that exhibit reflections of V_R in the waveguide. It is assumed that the waveguide coupler is placed between the accelerating cavity and the reflective element Γ_r . The directional coupler is supposed to have infinite directivity and $V_F = V_F^m$ and $V_R = V_R^m$. Also, the group delay τ_g of the signal from the cavity power coupler is reflected back at $\Gamma_r \in \mathbb{C}$ is

$$\tau_g \ll \frac{1}{\omega_{1/2}}. \quad (\text{A.1})$$

With (A.1) the field inside the waveguide can be approximated as being in steady state with respect to the accelerating field of the RF cavity. Therefore it is possible to define V_F

$$V_F = V_{F0} + rV_R \quad (\text{A.2})$$

with

$$r = \Gamma_r e^{j\omega_0 \tau_g} \quad (\text{A.3})$$

$r \in \mathbb{C}$ represents the fraction and the phase of the field that comes from the reflective element back to the cavity coupler. V_{F0} is the part of the forward signal that is generated by the RF amplifier. Using (A.2) with (6)

$$V_F = V_{F0} + r(V_P - V_F) \rightarrow V_F = V_P \frac{r}{r+1} + \frac{V_{F0}}{r+1}. \quad (\text{A.4})$$

The forward signal derived in (A.4) can be substituted in the cavity equations in (18)

$$\frac{dV_P}{dt} = -(\omega_{1/2} + j\Delta\omega + \frac{r}{r+1})V_P + 2\omega_{1/2} \frac{V_{F0}}{r+1} = \quad (\text{A.5})$$

$$= -(\omega_{1/2}^* + j\Delta\omega^*)V_P + 2\omega_{1/2}^*V_F^*, \quad (\text{A.6})$$

with the values of the equivalent resonant system identified by the asterisk (*). It is easy to see that the presence of r modifies the system detuning and bandwidth by a constant factor

$$\omega_{1/2}^* = \omega_{1/2} + \mathbb{R}\left\{\frac{r}{r+1}\right\}, \quad (\text{A.7})$$

$$\Delta\omega^* = \Delta\omega + \mathbb{I}\left\{\frac{r}{r+1}\right\}, \quad (\text{A.8})$$

$$V_F^* = \frac{\omega_{1/2}}{\omega_{1/2}^*(1+r)}V_{F0}. \quad (\text{A.9})$$

Since V_F^* is proportional to V_{F0} , it is equal to zero during the decay period. Therefore, if the system described in (A.6) is calibrated with the energy constrained method, (6) requires

$$V_P = V_F + V_R = V_F^* + V_R^*. \quad (\text{A.10})$$

Using (A.10) with (A.2) and (A.9) gives a linear transformation from the original cavity signals to the equivalent cavity model which comprises the effect of the reflective element

$$\begin{cases} V_F^* = q(V_F - rV_R), \\ V_F^* + V_R^* = V_F + V_R, \end{cases} \rightarrow \quad (\text{A.11})$$

$$\begin{cases} V_F^* = qV_F - qrV_R & = a^*V_F + b^*V_R, \\ V_R^* = (1-q)V_F + (1+rq)V_R & = c^*V_F + d^*V_R, \end{cases} \quad (\text{A.12})$$

with

$$q = \frac{\omega_{1/2}}{\omega_{1/2}^*(1+r)}. \quad (\text{A.13})$$

Therefore (A.12) describes the calibration with parameters a^*, b^*, c^*, d^* of the equivalent system with half bandwidth $\omega_{1/2}^*$.

Appendix B. Implementation of the calibration methods in python

Here the code for the diagonal, energy methods, and the one from Pfeiffer et al. used in the paper is given. The decay traces in the *calibrate* energy function have to be assigned to use the energy-constrained method.

```

2
1
2 # Copyright 2024 A. Bellandi et al.
3
4 # Permission is hereby granted, free of charge, to any person obtaining a copy of this
5 # software and associated documentation files (the "Software"), to deal in the Software
6 # without restriction, including without limitation the rights to use, copy, modify,
7 # merge, publish, distribute, sublicense, and/or sell copies of the Software, and to
8 # permit persons to whom the Software is furnished to do so, subject to the following
9 # conditions:
10
11 # The above copyright notice and this permission notice shall be included in all
12 # copies or substantial portions of the Software.
13
14 # THE SOFTWARE IS PROVIDED "AS IS", WITHOUT WARRANTY OF ANY KIND, EXPRESS
15 # OR IMPLIED,
16 # INCLUDING BUT NOT LIMITED TO THE WARRANTIES OF MERCHANTABILITY, FITNESS
17 # FOR A
18 # PARTICULAR PURPOSE AND NONINFRINGEMENT. IN NO EVENT SHALL THE AUTHORS
19 # OR COPYRIGHT
20 # HOLDERS BE LIABLE FOR ANY CLAIM, DAMAGES OR OTHER LIABILITY, WHETHER IN
21 # AN ACTION
22 # OF CONTRACT, TORT OR OTHERWISE, ARISING FROM, OUT OF OR IN CONNECTION
23 # WITH THE
24 # SOFTWARE OR THE USE OR OTHER DEALINGS IN THE SOFTWARE.
25
26
27 # Params
28
29 # hbw: Cavity half bandwidth in angular frequency
30 # probe_cmplx, vforw_cmplx, vrefl_cmplx: Cavity signal traces in I (real) and Q (imaginary)
31 # vforw_cmplx_decay, vrefl_cmplx_decay: Cavity signals at decay
32 # probe_amp_deriv: time derivative of the probe amplitude
33 # probe_sq_deriv: time derivative of the probe square amplitude
34 # kadd: tuning parameter
35
36 # The calibration algorithms returns a 4 complex values array with
37 #
38 # (a, b, c, d) = (arr[0], arr[1], arr[2], arr[3])
39
40 import numpy as np
41 from scipy.optimize import least_squares, lsq_linear
42

```

```

43 # ----- Utility functions -----
44
45 def C2RE(x):
46     """
47     Separate the real (even indices) from imaginary (odd indices) parts
48     of a complex array in a real array
49     """
50     result = np.empty(2 * np.array(x).shape[0], dtype=float)
51     result[0::2] = np.real(x)
52     result[1::2] = np.imag(x)
53     return result
54
55 def RE2C(x):
56     """
57     Merge the real (even indices) and imaginary (odd indices) parts
58     of a real array in a complex array
59     """
60     x = np.array(x)
61     return x[0::2] + 1.0j * x[1::2]
62
63 # ----- Calibration methods -----
64
65 def calibrate_diagonal(probe_cmplx, vforw_cmplx, vrefl_cmplx):
66     """
67     Classical calibration method. b,c terms are assumed to be zero and
68     probe = a*vforw + d*vrefl
69     """
70     A = np.empty((probe_cmplx.shape[0], 2), dtype=complex)
71     A[:, 0] = vforw_cmplx
72     A[:, 1] = vrefl_cmplx
73
74     b = probe_cmplx
75     calib = lsq_linear(A, b).x
76
77     return np.array([calib[0], 0.0, 0.0, calib[1]])
78
79 def calibrate_from_ref7_kadd_1(probe_cmplx, vforw_cmplx, vrefl_cmplx,
80                                probe_cmplx_decay, vforw_cmplx_decay, vrefl_cmplx_decay, kadd=1):
81     """
82     Method from:
83     Pfeiffer, Sven, et al. "Virtual cavity probe generation using calibrated
84     forward and reflected signals." MOPWA040, IPAC, 2015, 15.
85     The parameter 'kadd' is defaulted to 1
86     """
87     zeros = np.zeros_like(vforw_cmplx_decay)
88
89     A_probe = np.column_stack([vforw_cmplx, vrefl_cmplx] * 2)
90     A_vforw_cmplx_decay = np.column_stack([vforw_cmplx_decay, vrefl_cmplx_decay, zeros, zeros])
91     A_vrefl_cmplx_decay = np.column_stack([zeros, zeros, vforw_cmplx_decay, vrefl_cmplx_decay])
92
93     (x, _, _, y) = tuple(calibrate_diagonal(probe_cmplx, vforw_cmplx, vrefl_cmplx))
94
95     S = lsq_linear(np.column_stack([ -vrefl_cmplx_decay]), vforw_cmplx_decay).x[0]
96
97     Wb = np.abs(S)
98     Wc = kadd*Wb
99
100     A_absx = np.column_stack([np.abs(x)-Wc, [0.0], [1.0/Wc], [0.0]])
101     A_absy = np.column_stack([ [0.0], [1.0/Wb], [0.0], [np.abs(y)-Wb] ])
102
103     A = np.vstack([A_probe, A_vforw_cmplx_decay, A_vrefl_cmplx_decay, A_absx, A_absy])
104     b = np.concatenate([probe_cmplx, zeros, probe_cmplx_decay, [np.abs(x)], [np.abs(y)]])
105
106     return lsq_linear(A, b).x
107
108 def calibrate_brandt(hbw, probe_cmplx, vforw_cmplx, vrefl_cmplx, probe_amp_deriv,
109                     probe_cmplx_decay, vforw_cmplx_decay, vrefl_cmplx_decay):
110     """
111     Method from:
112     Brandt, Alexander. "Development of a Finite State Machine for the Automated
113     Operation of the LLRF Control at FLASH." No. DESY-THESIS---2007-024.
114     Deutsches Elektronen-Synchrotron (DESY), 2007.
115     """
116     (x, _, _, y) = tuple(calibrate_diagonal(probe_cmplx, vforw_cmplx, vrefl_cmplx))
117
118     z = lsq_linear(np.column_stack([vforw_cmplx_decay]), -vrefl_cmplx_decay).x[0]
119
120     probe_cmplx_conj_norm = np.conjugate(probe_cmplx) / np.abs(probe_cmplx)
121     opt_constant = probe_amp_deriv + np.abs(probe_cmplx) * hbw
122
123     # Calibrates b',c and d in function of a
124     def brandt_condition(a):
125         b = a/z
126         c = x-a
127         d = y-b
128         return (a, b, c, d)
129
130     # Optimization routine. The least squares method tries to minimize ||fun(a)||
131     def fun(a):
132         a = RE2C(a)[0]
133         abcd = brandt_condition(a)
134         vforw_calib = abcd[0] * vforw_cmplx + abcd[1] * vrefl_cmplx
135         dE = opt_constant - 2 * hbw * np.real(probe_cmplx_conj_norm * vforw_calib)
136
137         return C2RE(dE)
138
139     # The initial guess for the least squares algorithm is a=x
140     return brandt_condition(RE2C(least_squares(fun, C2RE(x)), method="lm").x)[0])
141
142 def calibrate_energy(hbw, probe_cmplx, vforw_cmplx, vrefl_cmplx, probe_sq_deriv,
143                     vforw_cmplx_decay=None, vrefl_cmplx_decay=None):
144     """
145     Cavity stored energy-based calibration method.
146     If the decay traces are assigned, the algorithm imposes a zero forward
147     in the decay phase.
148     """
149

```



```

155
156
157 max_probe_recip = 1.0/np.max(np.abs(probe_cmplx))
158 probe_cmplx_conj = np.conjugate(probe_cmplx)
159 C = probe_sq_deriv/(2 * hbw)
160 D = C + np.abs(probe_cmplx) ** 2
161
162 if (vforw_cmplx_decay is None or vrefl_cmplx_decay is None):
163     vforw_cmplx_decay = np.zeros(0)
164     vrefl_cmplx_decay = np.zeros(0)
165
166 # Optimization routine. The least squares method tries to minimize ||fun(abcd)||
167 def fun(abcd):
168     abcd = RE2C(abcd)
169     vforw_calib = abcd[0] * vforw_cmplx + abcd[1] * vrefl_cmplx
170     vrefl_calib = abcd[2] * vforw_cmplx + abcd[3] * vrefl_cmplx
171
172     vforw_calib_decay = abcd[0] * vforw_cmplx_decay + abcd[1] * vrefl_cmplx_decay
173
174     # Error of (6)
175     dprobe = vforw_calib + vrefl_calib - probe_cmplx
176
177     # Error of (19)
178     dD = (2.0 * np.real(probe_cmplx_conj * vforw_calib) - D) * max_probe_recip
179
180     # Error of (20)
181     dC = (np.abs(vforw_calib) ** 2 - np.abs(vrefl_calib) ** 2 - C) * max_probe_recip
182
183     # Error of (8)
184     dvforw_calib_decay = vforw_calib_decay
185
186     return C2RE(np.concatenate([dprobe, dD, dC, dvforw_calib_decay]))
187
188 # The initial guess for the least squares algorithm is (a=1, b=0, c=0, d=1)
189 return RE2C(least_squares(fun, C2RE([1.0, 0.0, 0.0, 1.0]), method='lm').x)

```

References

- [1] H. Padamsee, J. Knobloch, T. Hays, RF superconductivity for accelerators, John Wiley & Sons, 2008.
- [2] J. Branlard, V. Ayvazyan, O. Hensler, H. Schlarb, C. Schmidt, et al., Superconducting cavity quench detection and prevention for the European XFEL, in: Proc. 16th Int. Conf. RF Superconductivity, SRF'16, 2013, pp. 1239–1241.
- [3] R. Brinkmann, et al., The European XFEL project, in: FEL, 6, 2006, p. 24.
- [4] A. Neumann, W. Anders, O. Kugeler, J. Knobloch, Analysis and active compensation of microphonics in continuous wave narrow-bandwidth superconducting cavities, Phys. Rev. Special Topics-Accelerators Beams 13 (8) (2010) 082001.
- [5] R. Rybaniec, V. Ayvazyan, J. Branlard, S.P. Butkowski, H. Schlarb, C. Schmidt, G.W. Cichalewski, K. Przygoda, Ł. DMCS TUL, Real-time estimation of superconducting cavities parameters, in: Proc. 5th Int. Particle Accelerator Conf., 2014, pp. 2456–2458.
- [6] A. Bellandi, Ł. Butkowski, B. Dursun, A. Eichler, Ç. Gümüş, M. Kuntzsch, A. Nawaz, S. Pfeiffer, H. Schlarb, C. Schmidt, et al., Online detuning computation and quench detection for superconducting resonators, IEEE Trans. Nucl. Sci. 68 (4) (2021) 385–393.
- [7] S. Pfeiffer, V. Ayvazyan, J. Branlard, L. Butkowski, R. Rybaniec, H. Schlarb, C. Schmidt, R. Rybaniec, Virtual cavity probe generation using calibrated forward and reflected signals, in: Proc. 6th Int. Particle Accelerator Conf., 15, 2015, pp. 200–202.
- [8] A. Brandt, Development of a Finite State Machine for the Automated Operation of the LLRF Control at FLASH, (Ph.D. thesis), Deutsches Elektronen-Synchrotron (DESY), Universität Hamburg, 2007.
- [9] R. Penrose, On best approximate solutions of linear matrix equations, in: Mathematical Proceedings of the Cambridge Philosophical Society, 52, Cambridge University Press, 1956, pp. 17–19.
- [10] K. Zenker, C. Gümüş, M. Hierholzer, P. Michel, S. Pfeiffer, H. Schlarb, C. Schmidt, R. Schurig, R. Steinbrück, M. Kuntzsch, MicroTCA. 4-based low-level RF for continuous wave mode operation at the ELBE accelerator, IEEE Trans. Nucl. Sci. 68 (9) (2021) 2326–2333.
- [11] F. Qiu, J. Ma, G. Jiang, Z. Xue, Z. Zhu, L. Shi, T. Jiang, K. Jin, Q. Chen, C. Xu, et al., Approach to calibrate actual cavity forward and reflected signals for continuous wave-operated cavities, Nucl. Instrum. Methods Phys. Res. A 1034 (2022) 166769.
- [12] T. Schilcher, Vector sum control of pulsed accelerating fields in Lorentz force detuned superconducting cavities, in: Tech. rep., DESY Hamburg, Germany, 1998.
- [13] P. Virtanen, R. Gommers, T.E. Oliphant, M. Haberland, T. Reddy, D. Cournapeau, E. Burovski, P. Peterson, W. Weckesser, J. Bright, S.J. van der Walt, M. Brett, J. Wilson, K.J. Millman, N. Mayorov, A.R.J. Nelson, E. Jones, R. Kern, E. Larson, C.J. Carey, Í. Polat, Y. Feng, E.W. Moore, J. VanderPlas, D. Laxalde, J. Perktold, R. Cimrman, I. Henriksen, E.A. Quintero, C.R. Harris, A.M. Archibald, A.H. Ribeiro, F. Pedregosa, P. van Mulbregt, SciPy 1.0 Contributors, SciPy 1.0: Fundamental Algorithms for Scientific Computing in Python, Nature Methods 17 (2020) 261–272, <http://dx.doi.org/10.1038/s41592-019-0686-2>.
- [14] B. Aune, R. Bandelmann, D. Bloess, B. Bonin, A. Bosotti, M. Champion, C. Crawford, G. Deppe, B. Dwersteg, D. Edwards, et al., Superconducting TESLA cavities, Phys. Rev. Special Topics-accelerators Beams 3 (9) (2000) 092001.
- [15] R.W. Schafer, On the frequency-domain properties of Savitzky-Golay filters, in: 2011 Digital Signal Processing and Signal Processing Education Meeting (DSP/SPE), IEEE, 2011, pp. 54–59.
- [16] J. Branlard, V. Ayvazyan, A. Bellandi, J. Eschke, C. Gümüş, D. Kostin, K. Przygoda, H. Schlarb, J. Sekutowicz, Status of cryomodule testing at CMTB for CW R&D, in: Proc. 19th Int. Conf. RF Superconductivity, SRF'19, 2019, pp. 1129–1132.